Structure and phase behavior of square-well dimer fluids

Mark P. Taylor,[a] Jutta Luettmer-Strathmann,[b] and J. E. G. Lipson[c]
Department of Chemistry, Dartmouth College, Hanover, New Hampshire 03755

(Received 1 May 2000; accepted 15 November 2000)

A Born–Green–Yvon integral equation approach is used to study the structure and phase behavior of a fluid of fused square-well-sphere dimers. We compute site–site distribution functions for dimers with bond lengths of $L=0.6\sigma$, 0.8σ, and 1.0σ (where σ is the hard-sphere diameter) and square-well diameters ranging from $\lambda=1.25\sigma$ to 2.0σ over a wide range of temperature and density, and make comparisons with both exact and simulation results. For the tangent square-well dimer fluid having $\lambda=1.5$ we obtain a binodal and spinodal via the energy route, and compare our results with Monte Carlo data. The computational intensity of this approach has lead us to search for an alternate route to information about phase behavior, and so we also show how our compressibility results may be used in order to construct approximate spinodal curves. © *2001 American Institute of Physics.* [DOI: 10.1063/1.1338981]

I. INTRODUCTION

In recent work we have been using the Born–Green–Yvon (BGY) integral equation theory[1,2] in order to satisfy a long-range goal of constructing a theoretical treatment for continuum polymeric fluids, their solutions and mixtures. To this end we have previously derived the BGY results for hard-sphere-dimer[3] and flexible hard-sphere-chain and ring polymer fluids[4,5] as well as for an isolated square-well chain[6] and ring.[7] Here we extend our work using the square-well potential and present results for fluids of square-well dimers. The square well potential has had a continuing presence in the literature and has recently been used both in simulation and theoretical studies in order to model *n*-alkanes,[8,9] and also in simulations on mixtures.[10–13] While the isotropic square-well potential is relatively unsophisticated, square-well fluids and mixtures are capable of exhibiting all of the interesting phase behavior associated with real fluids and fluid mixtures. This fact, and the availability of simulation data for square-well systems, makes the square-well potential a reasonable starting point in shifting from a hard-sphere potential to one with an attractive component.

In our studies on molecular fluids we employ a so-called interaction site model in which the molecules are ''built'' from spherically symmetric simple-fluid monomers (in our work so far these are hard or square-well spheres). This approach is particularly valuable when dealing with flexible molecules such as linear polymer chains. A full molecule–molecule description of a polymer liquid would be extremely cumbersome and not particularly useful. The simpler site–site description is, however, both manageable and provides a great deal of information about the structure and thermodynamics of a polymer fluid.

In general, the microscopic structure of an isotropic liquid is described in terms of a pair or two particle correlation function.[14,15] For simple monatomic fluids, this function gives the probability of finding two particles separated by a given distance and is known as the radial distribution function. In the case of molecular fluids, the two particle distribution function contains information about both positional and orientational correlations between molecules and is thus, no longer a simple radially symmetric function. In either case, the full two particle correlation function is sufficient to determine the thermodynamic properties of the liquid. However, the task may be simplified by the use of the set of site–site distribution functions, which describe positional correlations between specific atoms comprising the molecules. These radially symmetric site–site functions are easier to calculate than the full molecule–molecule distribution function and can be directly probed in x-ray and neutron scattering experiments. Although they contain less information than the full molecular pair distribution function, these site–site functions are sufficient to calculate many thermodynamic properties of the molecular fluid.

In this work we present results for both structural and thermodynamic properties of several square-well dimer systems and test our theory via comparison with a variety of recent exact[16] and simulation results.[17–21] The results presented here are a first step towards using the BGY theory to calculate the structural and thermodynamic properties of flexible square-well-chain polymer liquids, as well as the properties of simple mixtures.

II. THEORY

A. The model fluid

In this work we study the structure and thermodynamics of a fluid of diatomic interaction site molecules. The fluid is composed of N molecules in a volume V at temperature T. The molecules have fixed bond length L and the sites of the ith molecule, labeled i and i', are located by the vectors $\vec{r}_i$ and $\vec{r}_{i'}$ (where $r_{ii'}=|\vec{r}_i-\vec{r}_{i'}|=L$). The potential between any two sites i and j on different molecules is $u_{ij}=u(r_{ij})$ and

[a]Current address: Department of Physics and Astronomy, Swarthmore College, Swarthmore, PA 19081.
[b]Current address: Department of Physics, University of Akron, Akron, OH 44325.
[c]Author to whom correspondence should be addressed.

the total interaction between two molecules is simply the sum of the site–site potentials $U_{ij}=u_{ij}+u_{i'j}+u_{ij'}+u_{i'j'}$. In this work we specialize to the case of square-well interaction sites, although the formalism developed here can be applied to any spherically symmetric potential. The site–site square-well potential is given by

$$u_{ij}=u(r_{ij})=\begin{cases}\infty, & 0<r_{ij}<\sigma,\\ -\epsilon, & \sigma\leqslant r_{ij}\leqslant\lambda\sigma,\\ 0, & r_{ij}>\lambda\sigma,\end{cases} \tag{1}$$

where σ is the hard-core diameter, λ is the square-well diameter and $-\epsilon$ is the well depth. We consider only the cases where $L<\sigma$ and $\lambda<\sigma+L$. The hard-core molecular volume is given by $v_m=(\pi/6)\rho\sigma^3[1+1.5(L/\sigma)-0.5(L/\sigma)^3]$.

B. The site–site BGY equation

The structure of this diatomic fluid can be described in terms of a spherically symmetric site–site distribution function $g(r_{12})$ which is proportional to the probability density that any two sites on different molecules will be separated by a distance r_{12}. As we have shown previously,[3] one can construct an exact integral equation for this site–site distribution function following the approach of Born, Green, and Yvon. The resulting site–site BGY equation is given by

$$\begin{aligned}\vec{\nabla}_1 g_{12}=&\vec{\nabla}_1[-\beta u_{12}]g_{12}+\int d\vec{r}_{1'}\, s_{11'}\vec{\nabla}_{1'}[-\beta u_{1'2}]g_{11'2}\\ &+\int d\vec{r}_{2'}\, s_{22'}\vec{\nabla}_1[-\beta u_{12'}]g_{122'}\\ &+\int d\vec{r}_{1'}\, s_{11'}\int d\vec{r}_{2'}\, s_{22'}\vec{\nabla}_{1'}[-\beta u_{1'2'}]g_{11'22'}\\ &+2\rho\int d\vec{r}_3\,\vec{\nabla}_1[-\beta u_{13}]g_{123}\\ &+2\rho\int d\vec{r}_3\int d\vec{r}_{1'}\, s_{11'}\vec{\nabla}_{1'}[-\beta u_{1'3}]g_{11'23},\end{aligned} \tag{2}$$

where $\beta=1/k_BT$, $\rho=N/V$, $s_{ii'}=\delta(r_{ii'}-L)/(4\pi L^2)$ is the dimer intramolecular distribution function and $g_{11'2}, g_{11'23}$, etc., are two and three molecule multisite distribution functions. This BGY equation can be associated with the physical process of perturbing molecule 1 from its equilibrium position and computing the resultant restoring force acting on site 1 of molecule 1 due to a fixed site 2 on molecule 2 (averaged over all positions of sites $1'$ and $2'$) and due to all other molecules 3.

C. Superposition approximations

The above BGY equation for the two-molecule site–site distribution function g_{12} is exact; however, it requires knowledge of an additional set of two- and three-molecule multisite distribution functions. In order to obtain a workable theory, we must express these multisite distribution functions in terms of the desired two-site function. This can be accomplished[3] by first reducing the three-molecule, multisite distribution functions to products of two-molecule distribution functions using the following molecular Kirkwood superposition approximations (KSA):

$$g_{ijk}=g_{ij}g_{ik}g_{jk}, \tag{3}$$

$$g_{ii'jk}=g_{ii'j}g_{ii'k}g_{jk}. \tag{4}$$

After this reduction of the three-molecule functions, the two-molecule, multisite (i.e., greater than two-site) distribution functions are written in terms of site–site functions using the following normalized site–site superposition approximations (NSSA):

$$g_{ii'j}=\frac{g_{ij}g_{i'j}}{n_{ij}n_{i'j}}, \tag{5}$$

$$g_{ii'jj'}=\frac{g_{ij}g_{i'j}g_{ij'}g_{i'j'}}{m_{ij}m_{i'j}m_{ij'}m_{i'j'}}. \tag{6}$$

The three-site normalization function n_{ij} is the average value of $g_{i'j}$ for a fixed site–site separation r_{ij}, subject to the $i-i'$ bonding constraint and is given by

$$n_{ij}=\int d\vec{r}_{i'}s_{ii'}g_{i'j}\Big/\int d\vec{r}_{i'}s_{ii'}. \tag{7}$$

Similarly, the four-site normalization function m_{ij} is the average value of $g_{i'j'}$ for a fixed site–site separation r_{ij}, subject to the $i-i'$ and $j-j'$ bonding constraints and forbidding $i'-j$ and $i-j'$ overlaps and is given by

$$\begin{aligned}m_{ij}=&\int d\vec{r}_{i'}s_{ii'}\int d\vec{r}_{j'}s_{jj'}\theta_{i'j}\theta_{ij'}g_{i'j'}\Big/\\ &\int d\vec{r}_{i'}s_{ii'}\int d\vec{r}_{j'}s_{jj'}\theta_{i'j}\theta_{ij'},\end{aligned} \tag{8}$$

where $\theta_{i'j}=\theta(r_{i'j}-\sigma)$ is a unit step function which vanishes for $r_{i'j}<\sigma$ and is unity otherwise. The above set of superpositionlike closure relations has been found to work well in describing both hard-sphere dimer and hard-sphere flexible-chain fluids.[4,6]

D. Numerical solution

Inserting the above superpositionlike closure relations [Eqs. (3)–(6)] into the dimer BGY equation [Eq. (2)] we obtain, after some manipulation, the following:

$$\frac{d}{dr}[\ln g(r)+\beta u(r)]$$
$$=\frac{1}{2n(r)Lr^2}\int_{|r-L|}^{r+L} ds(r^2+s^2-L^2)\frac{d}{ds}[-\beta u(s)]\frac{g(s)}{n(s)}$$
$$+\frac{1}{4\pi m(r)L^2 r}\int_{|r-L|}^{r+L} ds\,\frac{g(s)}{m(s)}\int_{|s-L|}^{s+L} dw\,w\frac{d}{dw}[-\beta u(w)]\frac{g(w)}{m(w)}\int_0^{\pi} d\phi\, f(r,s,L,w,\phi)\frac{g(v_L)}{m(v_L)}$$
$$+\frac{2\pi\rho}{r^2}\int_0^{\infty} ds\frac{d}{ds}[-\beta u(s)]g(s)\int_{|r-s|}^{r+s} dt(r^2+s^2-t^2)t\,g(t)$$
$$+\frac{2\rho}{n(r)Lr}\int_0^{\infty} ds\frac{g(s)}{n(s)}\int_{|r-s|}^{r+s} dt\,tg(t)\int_{|s-L|}^{s+L} dw\,w\frac{d}{dw}[-\beta u(w)]\frac{g(w)}{n(w)}\int_0^{\pi} d\phi\, f(r,s,t,w,\phi)\frac{g(v_t)}{n(v_t)}, \tag{9}$$

where

$$v_t^2=t^2+w^2-2tw[xz_t+[(1-x^2)(1-z_t^2)]^{1/2}\cos\phi], \tag{10}$$

$$f(r,s,t,w,\phi)=xy_t-[(1-x^2)(1-y_t^2)]^{1/2}\cos\phi, \tag{11}$$

$$x=\frac{s^2+w^2-L^2}{2sw},\quad y_t=\frac{s^2+r^2-t^2}{2sr},\quad z_t=\frac{s^2+t^2-r^2}{2st}, \tag{12}$$

and the normalization functions can be written as

$$n(r)=1+\frac{1}{2rL}\int_{|r-L|}^{r+L} ds\,s[g(s)-1], \tag{13}$$

$$m(r)=\begin{cases}1+\dfrac{[1+F(r)]^{-2}}{4\pi L^2 r}\displaystyle\int_{\sigma}^{r+L} ds\int_{|s-L|}^{s+L} dw\,w[g(w)-1][\pi-\phi_{\sigma}(r,s,w)], & r<\sigma+L,\\ 1+\dfrac{1}{2rL}\displaystyle\int_{|r-L|}^{r+L} ds\,s[n(s)-1], & r\geqslant\sigma+L,\end{cases} \tag{14}$$

where

$$F(r)=\frac{1}{4rL}[(r-L)^2-\sigma^2] \tag{15}$$

and

$$\phi_{\sigma}(r,s,w)=\cos^{-1}\left(\frac{w^2+L^2-\sigma^2-2wLxz_L}{2wL[(1-x^2)(1-z_L^2)]^{1/2}}\right). \tag{16}$$

The above definition of the angle $\phi_{\sigma}=\cos^{-1}$ (arg) is only valid for $|\text{arg}|<1$. For $\text{arg}<-1$, $\phi_{\sigma}=\pi$ and for $\text{arg}>1$, $\phi_{\sigma}=0$. For the square-well potential, defined in Eq. (1), the required derivative is

$$\frac{d}{dr}[-\beta u(r)]=\delta(r-\sigma^+)-(1-e^{-\beta\epsilon})\delta(r-\lambda\sigma), \tag{17}$$

where $\delta(r)$ is the Dirac delta function. This expression allows for analytic evaluation of one integral in each term on the right-hand side of Eq. (9). The latter equation is brought into a form suitable for numerical solution by integrating both sides over the variable r, from r to ∞, and noting that $g(r\to\infty)=1$. Finally, further manipulation, rewriting all long-ranged integrals over $g(r)$ in terms of $g(r)-1$, is advantageous.

The resulting equation has been solved numerically on a grid $1.0\leqslant r/\sigma\leqslant 25.0$ with $\Delta r=0.05\sigma$ using the standard Picard iteration method.[14] As usual in this type of iterative solution, the input $g(r)$ function for each iteration cycle is given by the output function of the previous cycle ''mixed'' with the input of the previous cycle. We use a mixing factor of 10%. Convergence is considered to have been achieved when the relative difference between the input and output functions is less that 10^{-6} for all grid points. All numerical integrations in the range $0.0\leqslant r/\sigma\leqslant 1.0$ are evaluated using 16-point Gaussian quadrature. The same technique is used for the ϕ integrations in Eq. (9) where the required $g(v)$, $n(v)$, and $m(v)$ values are determined via linear interpolation. All other numerical integrations are performed using Simpson's rule. Special care must be taken in handling these numerical integrals as the $g(r)$ function for square-well dimers is discontinuous (by a factor of $e^{\beta\epsilon}$) at $r=\lambda\sigma$ and possesses slope discontinuities at $r=\sigma+L$ and $r=\lambda\sigma+L$.[16]

We note that the solution presented here differs from our previous solution to the site–site BGY equation for hard-sphere dimers.[3] In that work we used a Legendre polynomial expansion of the $g(r)$ functions in order to deal with the ϕ integrations in Eq. (9). The solution given here is certainly more direct and, when applied to hard-sphere dimers (given

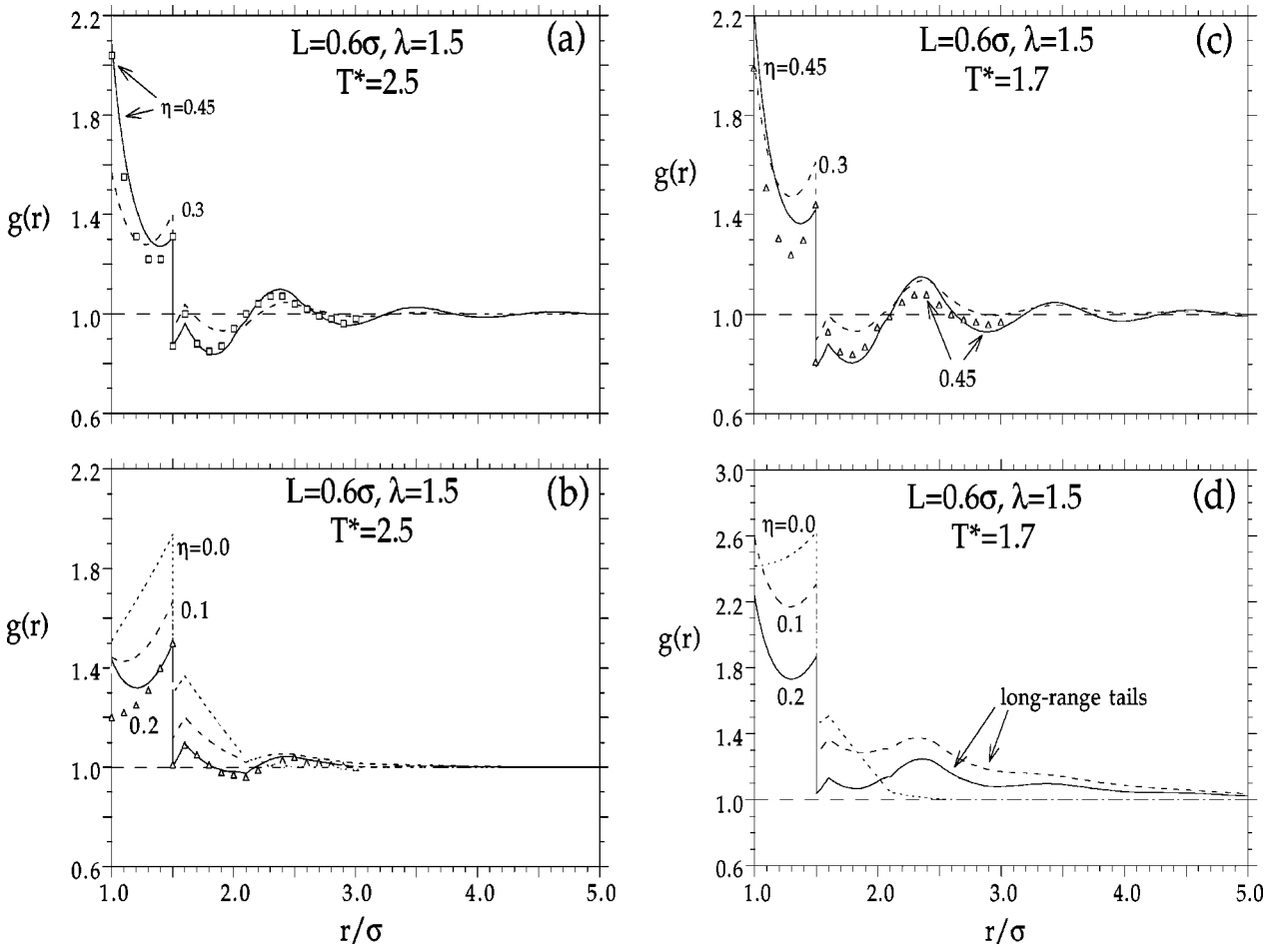

FIG. 1. Site–site distribution functions for square-well dimers with bond length $L=0.6\sigma$ and well diameter $\lambda=1.5$ at $T^*=2.5$ (a,b) and $T^*=1.7$ (c,d) for a range of volume fractions η. The lines are results from the BGY integral equation, the filled symbols are the exact $\eta=0$ results from Ref. 16 and the open symbols are MC results from Ref. 20. The critical point for this system is located at $T_c\approx 2.1$, $\eta_c\approx 0.15$.

by either the $\lambda=1$ or $\epsilon=0$ limits of the Eq. (1) square-well potential), reproduces our previous numerical results.

III. RESULTS

A. Structure

In Figs. 1 and 2 we show site–site distribution functions for $L=0.6\sigma$ and 1.0σ square-well dimers at two different temperatures ($T^*=1/\beta\epsilon$) for a series of dimer volume fractions $\eta=\rho v_m$, calculated using the site–site BGY equation. These distribution functions are discontinuous by a factor at e^{1/T^*} at the square-well boundary ($r=\lambda\sigma$) and display a cusp at $r=\sigma+L$ characteristic of hard-sphere molecular fluids. At low densities the contact value of the distribution functions display nonmonotonic behavior with increasing volume fraction due to a competition between the attractive square-well and the repulsive screening effects of the bonded site. At high density the distribution functions begin to resemble those of a monomeric square-well-sphere fluid. The BGY equation is seen to do a reasonably good job compared to the exact $\eta=0$ results,[16] both for $L=0.6\sigma$ and $L=1.0\sigma$, and the computer simulation results[20] for $L=0.6\sigma$ at $\eta=0.2$ and 0.45. At low temperatures and intermediate densities the BGY $g(r)$ functions display long range tails [see Figs. 1(d) and 2(d)] for which $g(r)>1$ out to large distances. A similar anomalous positive ''tailing'' has been observed previously in BGY results for the monomeric square-well-sphere fluid.[22] In the following we will associate this tailing behavior with an unstable fluid region.

B. Thermodynamics

A number of thermodynamic properties of the square-well-sphere dimer fluid can be computed from the site–site distribution function. In particular, the isothermal compressibility κ_T and excess internal energy $u^{\rm ex}$ are given directly as integrals over the site–site distribution function[14,15]

$$\rho\kappa_T/\beta=\frac{1}{\beta}\left(\frac{\partial\rho}{\partial P}\right)_T=1+4\pi\rho\int_0^\infty dr\, r^2[g(r)-1], \quad (18)$$

$$\beta u^{\rm ex}/N=-8\pi\rho(\beta\epsilon)\int_\sigma^{\lambda\sigma} dr\, r^2 g(r). \quad (19)$$

Either of these equations provides an alternate ''route'' to the thermodynamics of the system. For example, the pressure P can be computed via the compressibility route by integrating $1/\kappa_T$ with respect to density, as indicated in Eq. (18). The pressure can also be determined using the above energy

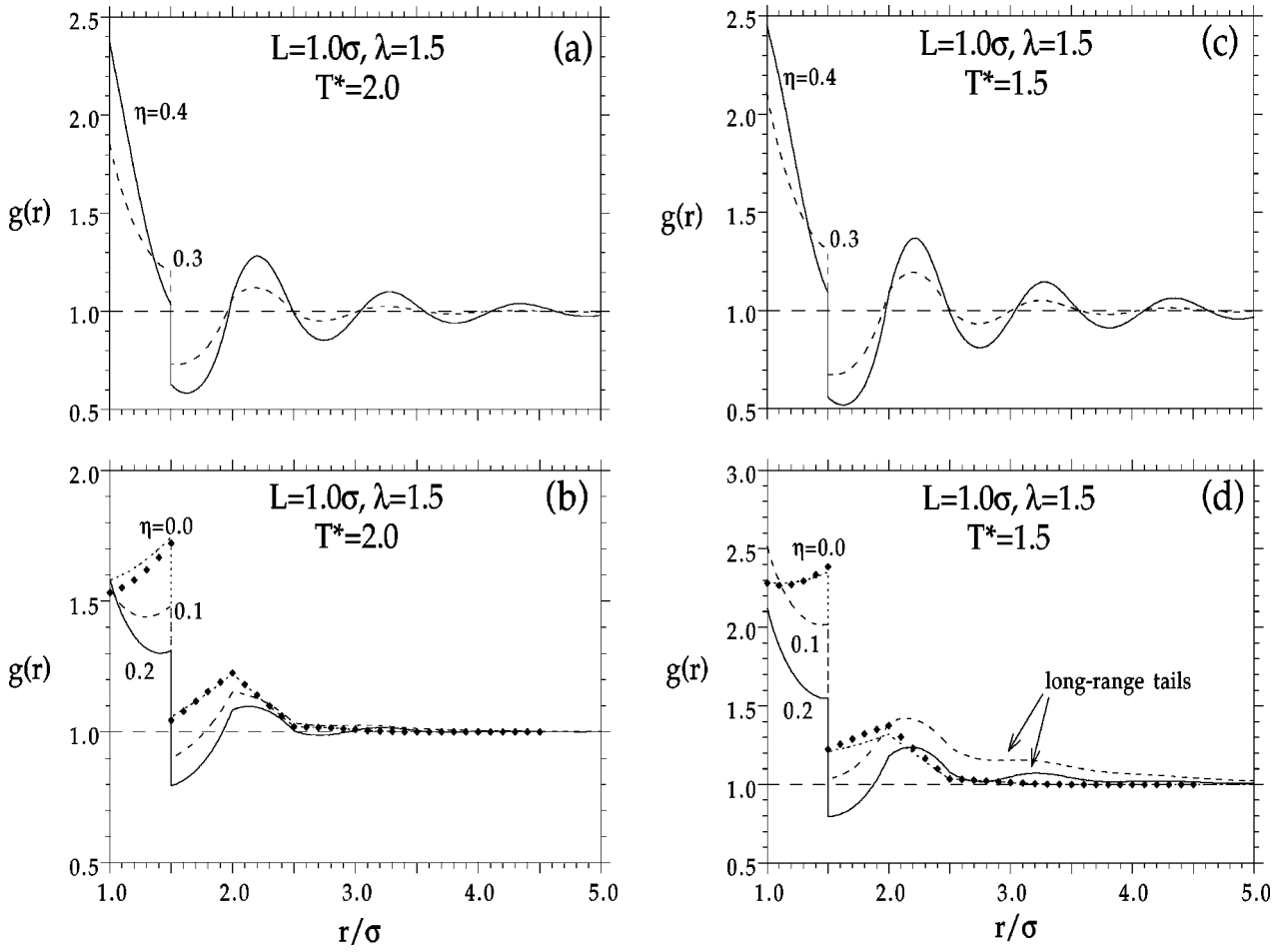

FIG. 2. Site–site distribution functions for square-well dimers with bond length $L=1.0\sigma$ and well diameter $\lambda=1.5$ at $T^*=2.0$ (a,b) and $T^*=1.5$ (c,d) for a range of volume fractions η. The lines are results from the BGY integral equation and the filled symbols are the exact $\eta=0$ results from Ref. 16. The critical point for this system is located at $T_c\approx 1.6$, $\eta_c\approx 0.14$. (Ref. 17).

equation [Eq. (19)]. In this route one first determines the excess Helmholtz free energy A^{ex} by integrating the relation $u^{\mathrm{ex}}=[\partial(\beta A^{\mathrm{ex}})/\partial\beta]_V$ and then the excess pressure is given by $P^{\mathrm{ex}}=-(\partial A^{\mathrm{ex}}/\partial V)_T$.[14,23] The ''excess'' here is over the infinite temperature reference system which in this case is the hard-sphere dimer fluid, and thus, this route also requires information about the hard-core system. Finally, a third route to thermodynamics is provided by the virial equation, which for molecular fluids requires knowledge of a three-site distribution function ($g_{11'2}$ for dimers)[3] in addition to the two-site function g_{12}.[24,25] Details of this approach as applied to diatomics are given in Ref. 3.

In Fig. 3 we show the pressure, in terms of the so-called compressibility factor $\beta P/\rho$, for square-well dimers with $L=\sigma$ and $\lambda=1.5$ computed by all three routes mentioned above using the distribution functions from our BGY theory. For the energy route we use the Tildesley–Street expression for the pressure of the hard-sphere-dimer fluid[26] and for the virial route we use the Eq. (5) superposition approximation for the required three-site distribution function. In comparison with the simulation data included in this figure, the three routes are all accurate at low densities, the virial route slightly overestimates the pressure at intermediate densities, and all three routes underestimate the pressure at high densities, with the compressibility route performing the worst in the latter regime.

In the inset to Fig. 3 we show the dimensionless pressure $\beta P v_m$ as computed by the compressibility route alone, both above and below the critical temperature ($T_c\sim 1.6$) for the $L=\sigma$, $\lambda=1.5$ system. The striking plateau seen in the subcritical $T^*=1.5$ isotherm is very suggestive of phase separation. This plateau is due to very large compressibility values, shown in Fig. 4, which arise form the long-range tails in $g(r)$ [see in Fig. 2(d)]. Since there is no true divergence of κ_T in the model the subcritical pressure plateaus are not truly ''flat'' and thus do not rigorously demonstrate phase separation. However, we will use this compressibility behavior to construct approximate spinodal curves in part 2 of the next section. We note that the pressure isotherms computed from the energy route do develop a ''van der Waals loop'' as the temperature is lowered and thus phase separation is predicted. We compute the resulting energy route phase boundaries in part 1 of the next section. Finally, the virial pressure gives no indication of phase separation at low temperatures.

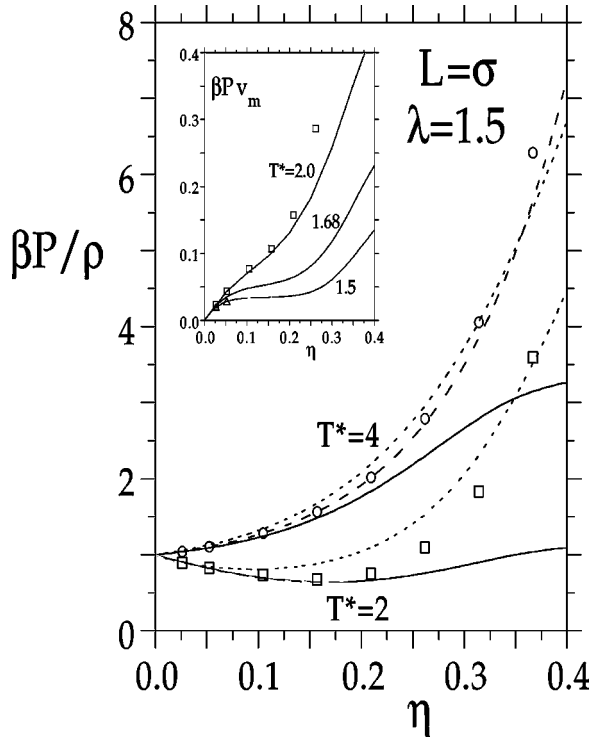

FIG. 3. Compressibility factor $\beta P/\rho$ for square-well dimers with $L=1.0\sigma$ and $\lambda=1.5$ at temperatures $T^*=2$ and 4 as indicated. The lines gives the BGY results as computed via the compressibility (—), energy (– – –), and virial (---) routes while the symbols are simulation results from Ref. 19. Inset: Dimensionless pressure $\beta P v_m$ for the same system at temperatures $T^*=2.0$, 1.68, and 1.5 as indicated. The lines are the BGY results from the compressibility route only and the symbols are simulation results as above. For the $T^*=1.5$ MC data, the two filled symbols lie within the two-phase region.

C. Phase behavior

1. Binodal and spinodal via the energy route

The energy route to the binodal involves calculation of the total Helmholtz free energy, which can be divided into two contributions: that associated with the square-well interaction and that with the hard-core fluid. Here we compute the hard-core contribution A^{hc} via analytical integration of the Tildesley–Street equation of state for tangent dimers.[26] The square-well contribution is determined from the BGY $g(r)$ results via numerical integration of the excess internal energy u^{ex} [where u^{ex} is obtained via numerical integration of Eq. (19)]. We note that $g(r)$ must be computed at a large number of (η,T)-state points (we use 144 points) to construct the full $A^{ex}(\eta,T)$ function. The total pressure and total chemical potential can then be obtained via differentiation of the total Helmholtz free energy $A^{tot}=A^{hc}+A^{ex}$, a procedure which is made easier by fitting $A^{ex}(\eta,T)$ to a cubic function of the volume fraction (η). The binodal is mapped out by plotting pressure versus chemical potential and locating the intersection points, while points on the spinodal are obtained directly using either the pressure or the chemical potential. The results are illustrated in Fig. 5, which shows the BGY energy-route binodal and spinodal for a tangent square-well dimer fluid having $\lambda=1.5$; the critical point is located at $T_c=1.724$ and $\eta_c=0.167$. Also included are the Monte Carlo data of Yethiraj and Hall,[27] associated with a critical point of $T_c=1.58$ and $\eta_c=0.146$.

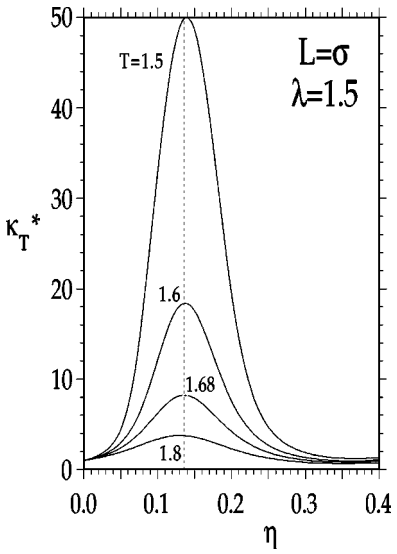

FIG. 4. BGY results for the reduced isothermal compressibility $\kappa_T^*=\rho\kappa_T/\beta$ for square-well dimers with bond length $L=1.0\sigma$ and well diameter $\lambda=1.5$. The BGY estimate of the critical point ($T_c\approx1.68$ $\eta_c\approx0.136$) is located by the dashed lines.

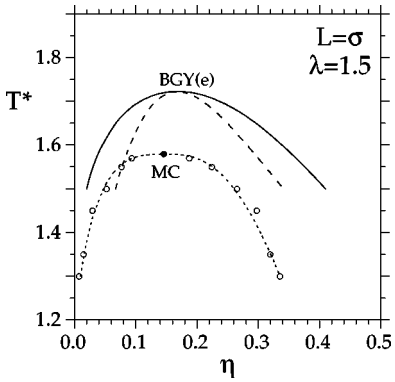

FIG. 5. Liquid–vapor phase diagram for square-well dimers with well diameter $\lambda=1.5$ and bond length $L=1.0\sigma$. The solid line is the BGY binodal obtained from the energy route, and the long-dashed curve is the corresponding BGY spinodal. The open symbols are Gibbs ensemble MC results (Ref. 17), and the dashed line is a fit to the MC data with the filled symbol locating the critical point.

2. Approximation of spinodal

The route described in the preceding section yields results for the binodal and spinodal which are comparable to those obtained for several recent methods, however, not as close to simulation results as the predictions of the generalized Flory dimer (GFD) theory, or RISM/MSA theory.[17] However, a more serious drawback to the route outlined in Sec. I is the effort required to obtain such a binodal. Given the large computational requirement involved even for dimers, and considering that our goal is to focus eventually on polymer fluids and mixtures, it would be desirable to have an alternate method. In this section we describe an approximation to the spinodal which makes use of our compressibility results. Our route is an indirect one, reflecting the fact that, while we observe a rise in the compressibility at low temperatures from both the low and high density sides, we

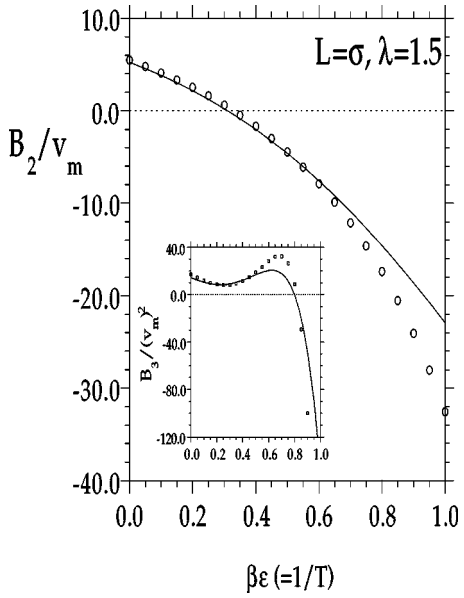

FIG. 6. Second and, in the inset, third virial coefficients for square-well dimers with bond length $L=1.0\sigma$ and well diameter $\lambda=1.5$. The solid lines are the results of the BGY calculation while the symbols are exact B_2 results (Ref. 16) and Monte Carlo B_3 results (Ref. 17).

do not find a divergent compressibility [which would in fact be impossible in our direct numerical calculation of $g(r)$]. The ''true'' spinodal may be mapped out as the set of points at which the compressibility diverges. Here we construct approximate spinodals by mapping out the loci of points in phase space which are associated with an anomalously large reduced compressibility $\kappa_{T*}=\rho\kappa_T/\beta$, using the distribution function at the critical point $g(r;\eta_c,T_c)$ to define a maximum reduced compressibility $\kappa_T^{\max}$. The set of all state points with $\kappa_T^*>\kappa_T^{\max}$ are considered ''anomalous'' and define the ''two-phase'' (or unstable) region of our approximate spinodal.

In order to carry out the above procedure we require an estimate of the critical temperature and density. We can obtain an estimate of the critical density from the volume fraction at which κ_T^* obtains a maximum value (see Fig. 4). Since the critical density for these square-well dimer systems is relatively low, a virial expansion approach can be used to determine the critical temperature. Here we density expand the distribution function as $g(r;\eta,T)=g_0(r;T)+\eta g_1(r;T)+O(\eta^2)$ and use the BGY equation to compute the expansion coefficients $g_0(r;T)$ and $g_1(r;T)$. This density expanded form of $g(r)$ is inserted into the above compressibility equation [Eq. (18)] to give the following three-term virial expansion of the pressure:

$$\beta P/\rho=1+\frac{B_2(T)}{v_m}\eta+\frac{B_3(T)}{v_m^2}\eta^2, \tag{20}$$

where v_m is the hard-core molecular volume. Second and third virial coefficients of square-well dimers with $L=\sigma$ and $\lambda=1.5$ computed from the BGY theory are compared in Fig. 6 with corresponding exact $B_2(T)$[16] and Monte Carlo $B_3(T)$ values.[17] These virial coefficients can be used directly to estimate a critical temperature and density through the fact

TABLE I. Critical temperature T_c and volume fraction η_c for several square-well dimer systems as determined by the present BGY calculation (via approximation of the spinodal) and estimated from Gibbs ensemble (MC) simulations (Refs. 17 and 20). [Using the energy route the BGY critical point is found to be $T_c=1.724$ and $\eta_c=0.167$ for $L=\sigma$ and $\lambda=1.5$].

	BGY			MC	
L/σ	λ	T_c	η_c	T_c	η_c
0.6	1.5	2.13	0.154	2.12	0.155
0.8	1.5	1.86	0.148	1.78	0.167
1.0	1.25	0.95	0.171		
1.0	1.5	1.68	0.136	1.58[a]	0.146[a]
1.0	1.75	2.65	0.116		
1.0	2.0	3.88	0.100		

[a]Reference 28.

that both the first and second density derivatives of the pressure vanish at the critical point.[28] For example, it is readily established that within the above three-term virial approximation the critical volume fraction is $\eta_c=[-v_m/B_2(T_c)]$ which, given an estimate of η_c, implicitly locates T_c. Thus our BGY results for κ_T^* and $B_2(T)$ are sufficient to locate η_c and T_c. Critical points of several square-well dimer systems determined in this way are given in Table I. In comparison with MC estimates for T_c and η_c, our BGY approach tends to slightly overestimate the critical temperature and underestimate the critical density, although our values are generally within 10% of the simulation results. We can also compare the critical point obtained from the energy route described in Sec. I with that obtained here: Recall that for the case of the tangent dimer having $\lambda=1.5$ the energy route yields $T_c=1.724$, $\eta_c=0.167$, compared to our estimate here of $T_c=1.68$ and $\eta_c=0.136$ and the Monte Carlo results of $T_c=1.58$ and $\eta_c=0.146$.[27]

Using the critical points given in Table I to define a maximum reduced compressibility $\kappa_T^{\max}$, we can construct approximate spinodal curves as described above. The procedure is illustrated in Fig. 4 where $\kappa_T^{\max}$ for the $L=1.0\sigma$, $\lambda=1.5$ system is indicated by the horizontal dashed line. All (η,T) state points lying above this line are considered ''unstable'' and an approximation of the spinodal boundary is then located by the intersection of this line with the compressibility curves for each subcritical temperature. Results for six different square-well dimer systems are shown in Figs. 7 and 8. Figure 7 illustrates the variation in phase behavior due to changing bond length for a fixed well diameter of $\lambda=1.5$. As the bond length is increased from $L=0.6\sigma$ to 1.0σ, the critical point moves to lower temperature and the phase envelope narrows. In comparison with the MC data for these $\lambda=1.5$ systems, the BGY theory is seen to do a very good job of locating the region of phase separation. As expected, the approximate spinodal lies well within the BGY prediction for the binodal. Figure 7 displays the effects on phase behavior due to changing well diameter for a fixed bond length of $L=1.0\sigma$. As the well diameter is narrowed from $\lambda=2.0$ to $\lambda=1.25$, the critical point moves to lower temperature and higher density and the phase envelope becomes markedly flattened. These changes in location and

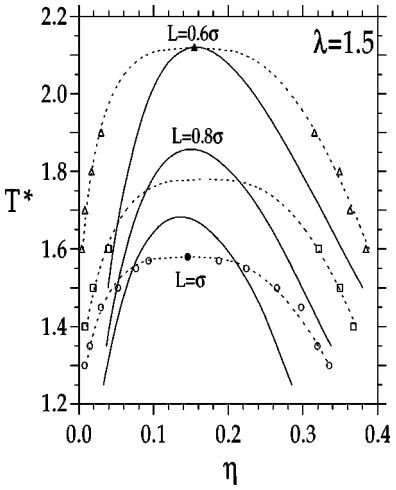

FIG. 7. Liquid–vapor phase diagram for square-well dimers with well diameter $\lambda = 1.5$ and bond lengths $L = 0.6\sigma$, 0.8σ, and 1.0σ, as indicated. The solid lines are the approximate spinodal curves obtained from the BGY integral equation and the open symbols are Gibbs ensemble MC results (Ref. 20 for $L = 0.6\sigma$, 0.8σ; Ref. 17 for $L = 1.0\sigma$). The dashed lines are fits to the MC data with the filled symbols locating the critical points.

shape of the $L = \sigma$ square-well dimer fluid phase boundaries are very similar to the behavior exhibited by square-well monomer fluids. Both the flattening of the phase envelope and the shift to lower temperature and higher density of the critical point are observed in the analogous monomeric system as the well diameter is decreased from $\lambda = 2.0$ to $\lambda = 1.25$.[27,29]

IV. DISCUSSION

This paper describes our results on the microscopic structure and phase behavior of a diatomic square-well fluid using the Born–Green–Yvon integral equation technique. We have compared our distribution functions with Monte Carlo data, and have computed a number of thermodynamic properties, including the pressure equation of state via three different routes. We have used the energy route to compute the binodal and spinodal diagrams for the tangent square-well dimer fluid having $\lambda = 1.5$. In addition, we have made use of our compressibility results in order to determine an approximate spinodal for a series of square-well dimer fluids associated with various bond lengths and well widths.

Our BGY predictions for $g(r)$ as a function of r, reduced temperature, density, and bond lengths show good agreement with the exact zero-density results and available simulation data. We used the $g(r)$ results in computing the compressibility factor for tangent square-well dimers having $\lambda = 1.5$ using three routes: compressibility, energy, and virial. While all routes are accurate at low densities, the agreement with simulation decreases with increasing density. This is particularly noticeable for the compressibility route. Using the free energy route we have obtained a binodal/spinodal diagram for this fluid which, while not as close to simulation results as the generalized Flory dimer or RISM/MSA theories,[17] is comparable to other recent theoretical treatments.[30,31] One advantage of the method described here is the extendibility to the case of long-chain fluids; however, it is clear that pursuing this standard route to the phase diagram will require significant computation resources, as well as accurate equation-of-state information about the associated hard-sphere fluid. We have therefore developed an alternate method which yields an approximation to the spinodal diagram. We located the critical point of the system (via a virial expansion) and took the isothermal compressibility at this point (which would be infinite for a real fluid) to be the maximal value possible for a stable phase. Our estimates of the critical temperature and density are generally within 10% of simulation results, with the BGY theory tending to overestimate these quantities. We identified state points considered to lie in the unstable, or two-phase, region as those associated with compressibilities exceeding this maximum value and thus mapped out approximate spinodal curves. The phase behavior predicted by this approximate method compared reasonably well with Gibbs ensemble MC results[28,29] for dimers having well diameter $\lambda = 1.5$ and bond length $L = 0.06\sigma$, 0.8σ, and 1.0σ.

In this work we have applied the BGY theory to the study of square-well dimer fluids, and have demonstrated that the theory is capable of capturing the physical behavior of such systems. We are in the process of applying the approach described in this paper to the case of longer square-well chain fluids. At that point we will be able to make connections with simulation results which use the square-well fluid to model *n*-alkanes.[31] Since our work using the lattice BGY theory has already been applied to study alkanes and alkane mixtures[32] this will allow us to make comparisons between the lattice and continuum results on analogous model fluids. In addition, having developed the continuum BGY theory for both hard-sphere and square-well fluids we will be in a position to initiate theoretical studies on simple mixtures, for which simulation results are also available.

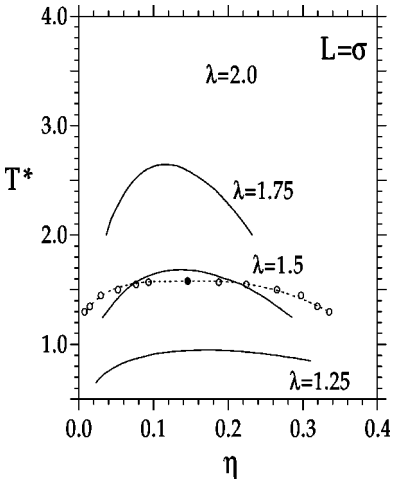

FIG. 8. Liquid–vapor phase diagram for square-well dimers with bond lengths $L = 1.0\sigma$, well diameters $\lambda = 2.0$, 1.75, 1.5, and 1.25, as indicated. The solid lines are the approximate spinodal curves obtained from the BGY integral equation, the open symbols for $\lambda = 1.5$ are Gibbs ensemble MC results (Ref. 17), and the dashed line is a fit to the MC data with the filled symbol locating the critical point.

ACKNOWLEDGMENT

Financial support from the National Science Foundation (DMR-9730976) is gratefully acknowledged.

[1] J. Yvon, Actual. Sci. Ind. **203**, (1935).
[2] M. Born and H. S. Green, Proc. R. Soc. London, Ser. A **188**, 10 (1946).
[3] M. P. Taylor and J. E. G. Lipson, J. Chem. Phys. **100**, 518 (1994).
[4] M. P. Taylor and J. E. G. Lipson, J. Chem. Phys. **102**, 2118 (1995).
[5] M. P. Taylor and J. E. G. Lipson, J. Chem. Phys. **102**, 6272 (1995).
[6] M. P. Taylor and J. E. G. Lipson, J. Chem. Phys. **104**, 4835 (1996).
[7] M. P. Taylor and J. E. G. Lipson, J. Chem. Phys. **106**, 5181 (1997).
[8] (a) H. Adidharma and M. Radosz, Fluid Phase Equilibria **160**, 165 (1999); **161**, 1 (1999).
[9] D. C. Williamson and Y. Guevara, J. Phys. Chem. B **103**, 7522 (1999).
[10] (a) G. McCabe, A. Gil-Villegas, and G. Jackson, Chem. Phys. Lett. **303**, 27 (1999); (b) J. Phys. Chem. B **102**, 4183 (1998).
[11] H. S. Gulati and C. K. Hall, J. Chem. Phys. **107**, 3930 (1997).
[12] H. L. Liu and Y. Hu, Fluid Phase Equilibria **138**, 69 (1997).
[13] D. R. Kuespert, V. Muralidharan, and M. D. Donohue, Mol. Phys. **86**, 201 (1995).
[14] J. P. Hansen and I. R. McDonald, *Theory of Simple Liquids* (Academic, London, 1986).
[15] C. G. Gray and K. E. Gubbins, *Theory of Molecular Fluids* (Clarendon, Oxford, 1984), Vol. 1.
[16] M. P. Taylor, Mol. Phys. **82**, 1151 (1994).
[17] A. Yethiraj and C. K. Hall, Mol. Phys. **72**, 619 (1991).
[18] A. Thomas and M. D. Donohue, Mol. Phys. **81**, 43 (1994).
[19] F. W. Tavares, J. Chang, and S. I. Sandler, Mol. Phys. **86**, 1451 (1995).
[20] M. Lisal and I. Nezbeda, Mol. Phys. **96**, 335 (1999).
[21] L. Hu, H. Rangwalla, J. Cui, and J. R. Elliot, Jr., J. Chem. Phys. **111**, 1293 (1999).
[22] K. D. Luks and J. J. Kozak, Adv. Chem. Phys. **37**, 139 (1978).
[23] C. Caccamo, Phys. Rev. Rep. **274**, 1 (1996).
[24] K. G. Honnell, C. K. Hall, and R. Dickman, J. Chem. Phys. **87**, 664 (1987).
[25] K. Schweizer and J. G. Curro, J. Chem. Phys. **89**, 3342 (1988).
[26] D. J. Tildesley and W. B. Street, Mol. Phys. **41**, 85 (1980).
[27] E. de Miguel, L. F. Rull, and K. E. Gubbins, Physica A **177**, 174 (1991).
[28] The critical point temperature and density are obtained from the MC coexistence data, as described in Ref. 20, by fitting to $\eta_l+\eta_v=2\eta_c+A(T_c-T)$ and $\eta_l-\eta_v=B(T_c-T)^{0.325}$, where η_l and η_v are the coexisting liquid and vapor volume fractions, respectively.
[29] L. Vega, E. de Miguel, and L. F. Rull, J. Chem. Phys. **96**, 2296 (1992).
[30] A. Gil-Villegas, A. Galindo, P. J. Whitehead, S. J. Mills, G. Jackson, and A. N. M. Burgess, J. Chem. Phys. **106**, 4168 (1997).
[31] F. W. Tavares, J. C. Chang, and S. I. Sandler, Fluid Phase Equilibria **140**, 129 (1997).
[32] J. Luettmer-Strathmann, J. A. Schoenhard, and J. E. G. Lipson, Macromolecules **31**, 9231 (1998).